Journal of ELECTRONIC MATERIALS, Vol. 49, No. 1, 2020
https://doi.org/10.1007/s11664-019-07787-2

Synthesis and Characterization of $LiCrO_2$ Thin Films As Potential Cathode Material for Lithium Ion Batteries

H.I. ELSAEEDY [1,2]

1.—Advanced Functional Materials and Optoelectronic Laboratory (AFMOL), Department of Physics, Faculty of Science, King Khalid University, P.O. Box 9004, Abha, Saudi Arabia. 2.—e-mail: halsayede@kku.edu.sa

Production of effective and inexpensive new material used as a cathode for lithium ion batteries is the main topic of this study. Thin films of lithium chromium oxide ($LiCrO_2$) were grown onto a glass substrate by spray pyrolysis using a chemical solution containing lithium acetate Li $(CH_3COO)_2$ and chromium trioxide (Cr_2O_3) as precursors. The depositions occurred in the substrate temperature range of 350°C. The investigation of the x-ray diffraction of the $LiCrO_2$ thin films was displayed to be polycrystalline with a rhombohedral structure. The linear optical parameters, represented in the refractive index, energy gap and absorption coefficient of the $LiCrO_2$ thin films were estimated via the transmittance and reflectance measurements. In the linear optical studies, the evaluated direct energy gaps of the $LiCrO_2$ thin films could be observed decreased by increasing the film thickness. The dispersion refractive index data of the $LiCrO_2$ thin films were analyzed according to the single oscillator model to evaluate the dispersion parameters including the dispersion energy, the optical dielectric constant and the oscillator energy. The nonlinear optical constants of the $LiCrO_2$ thin films were calculated.

Key words: Lithium chromium oxide, spray pyrolysis technique, x-ray diffraction, dispersion parameters, third-order nonlinear susceptibility

INTRODUCTION

Li-ion battery technology has received important attention in recent years where these batteries show great promise as power sources that can lead us to the electric vehicle (EV) revolution. The fabrication of new thin films based on lithium metal oxides to be used as a cathode for lithium-ion batteries (LIBs), micro-battery systems and microelectronic devices, are the main topics for many researchers in the field to fabricate new fascinating materials used in manufacturing such batteries.[1] Recently, lithium metal oxides $LiMO_2$ (M = Ni, Mn, Cr and Co) have been intensively explored as promising cathode materials for lithium-ion batteries, due to their high capacity, ease of preparation, nontoxicity and earth abundance.[2,3] These oxides generally demonstrate good chemical stability, high optical conductivity,[4] and high capacity.[5] Among these compounds, lithium chromium oxide $LiCrO_2$ is an important compound due to its high capacity and low price.[6] The fabrication of lithium metal oxides thin films was done by different techniques such as spray pyrolysis,[7] sol–gel,[8] hydrothermal,[9] magnetron sputtering,[10] and molten salt synthesis.[11] Previous studies demonstrated that chromium oxide has a good performance in the lithium ion batteries while the addition of lithium to the chromium oxide was studied at first time in this study. So, in this article we will fabricate $LiCrO_2$ thin films with thickness (162–381 nm) via an inexpensive spray pyrolysis technique at first time and study the structural properties of the $LiCrO_2$ thin films via XRD, FE SEM and EDAX analysis.

(Received August 24, 2019; accepted October 29, 2019; published online November 12, 2019)

Moreover, the linear and nonlinear optical properties of the $LiCrO_2$ films were evaluated and interpreted by recording the transmittance and reflectance data in the spectral range 400–2500 nm.

EXPERIMENTAL PROCEDURES

Growth of the $LiCrO_2$ Thin Films

Spray pyrolysis was employed exclusively for the synthesis of $LiCrO_2$ thin films. For the synthesis of $LiCrO_2$ thin films, different solutions of 0.5 M cadmium acetate Li $(CH_3COO)_2$ and 1 M of chromium trioxide (Cr_2O_3) were dissolved in deionized water. The $LiCrO_2$ solution was stirred at 50°C for about 1 h until a green color formed. The final $LiCrO_2$ solution was sprayed by spray pyrolysis onto a heated glass substrate. The substrate temperature was adjusted to be 350°C. The produced $LiCrO_2$ thin films exhibit a light green color. The thickness of the $LiCrO_2$ thin films was measured by alpha step D 500 stylus profilometer and it was found to vary in the range of 162–381 nm.

Characterization Techniques

The structural characterization of the $LiCrO_2$ thin films was analyzed by a Philips X' Pert diffractometer with CuKα radiation (λ = 1.540 Å).

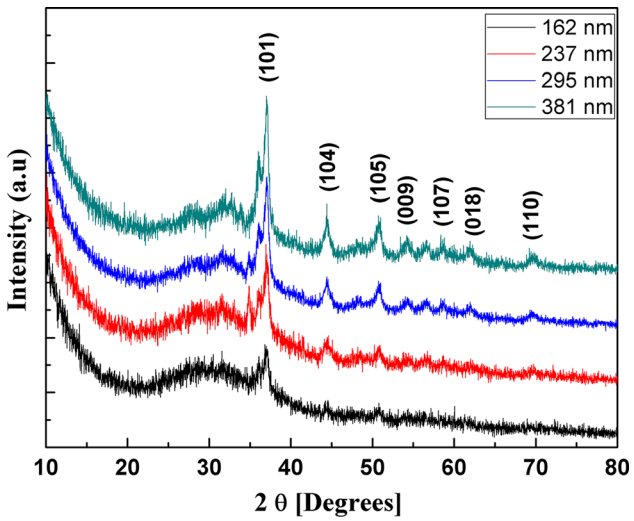

Fig. 1. The x-ray diffraction spectra for the $LiCrO_2$ thin films.

The linear and nonlinear optical calculations occurred by measuring both transmittance and reflectance for the $LiCrO_2$ thin films by spectrophotometer (kind JASCO Corp., V-570) in the range of 400–2500 nm.

RESULTS AND DISCUSSION

Structural Characterizations

XRD Analysis of $LiCrO_2$ Thin Film

Figure 1 displays the XRD spectra of the $LiCrO_2$ thin films. The XRD pattern indicates that $LiCrO_2$ films possess a polycrystalline nature. The diffraction peaks were matched fine with a rhombohedral structure conferring to JCPDS card No. 24-0600. It is noticed from the XRD pattern that all the observed peaks are from the $LiCrO_2$ only and there is no secondary phase.

The crystallite size (D) and the lattice strain (ε) of the $LiCrO_2$ films were estimated via the following Scherer expression [12,13]:

$$D = \frac{K\lambda}{\beta\cos(\theta)} \tag{1}$$

$$\varepsilon = \frac{\beta\cos(\theta)}{4} \tag{2}$$

where θ, β, ε are the Bragg diffraction angel, the experimental full width at the half maximum (FWHM) and the lattice strain. The magnitudes of the crystallites size (D) and the lattice strain (ε) for the $LiCrO_2$ films were recorded in Table I.

The dislocation density of the $LiCrO_2$ thin films was evaluated by [14,15]:

$$\delta = \frac{1}{D^2} \tag{3}$$

The values of the dislocation density (δ) of the $LiCrO_2$ films are tabulated in Table I. It is observed that the grain size increases while both the strain (ε) and the dislocation density (δ) of the $LiCrO_2$ thin films monotonically decrease upon the increase of thickness. Figure 2 presents the dependence of the crystallites size (D) and the strain (ε) on the film thickness for the $LiCrO_2$ films. By increasing the film thickness the crystallites size (D) increases and the strain (ε) decreases.

Table I. The structure parameters for the sprayed $LiCrO_2$ thin films

Film thickness, nm	D, nm	$\varepsilon \times 10^{-3}$	$\delta \times 10^{-4}$, nm^{-3}
162	58.73	6.19	2.89
237	49.42	7.23	4.09
295	42.75	9.95	5.46
381	37.69	14.01	7.04

The FE-SEM and Chemical Composition of $LiCrO_2$ Thin Film

The surface morphology and EDAX analysis of the $LiCrO_2$ thin films are represented in Fig. 3. The figure shows that the film's surface is smooth and uniform. EDAX analysis of the $LiCrO_2$ thin film displays the peaks of Cr and O found in the sample and the Li peak not observed in the EDAX pattern due to the x-ray fluorescence yield is extremely low for Li. The atomic ratio of Si, Cr and O are Si = 46.82, Cr = 17.62, O = 35.56 at.%.

Linear Optical Analysis

Figure 4a and b displays the spectral distribution of the transmission T and reflection R for the $LiCrO_2$ thin films. It obvious from the figure that the transmittance, T of the $LiCrO_2$ thin films was decreased by increasing the thickness while the reflectance, R was increased by increasing the film thickness.

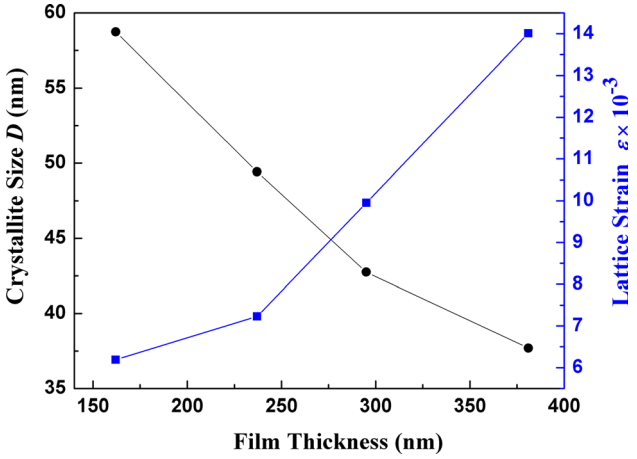

Fig. 2. The crystallite size and lattice strain as a function of the $LiCrO_2$ film thickness.

Linear Absorption Coefficient and Energy Gap Evaluation

The absorption coefficient, α of the $LiCrO_2$ thin films were estimated by knowing the transmission and reflection data of the $LiCrO_2$ films via the presented equation [16,17]:

$$\alpha = \frac{1}{t}\ln\left[\frac{(1-R)^2}{2T} + \left(\frac{(1-R)^4}{4T^2} + R^2\right)^{1/2}\right] \quad (4)$$

where t represents the value of film thickness and K represents the absorption index of the $LiCrO_2$ films.

Figure 5a represents the spectral variant of the absorption coefficient of the $LiCrO_2$ films with the wavelength. It is obvious from this plot that the absorption coefficient decreases as wavelength decreases, additionally, there is an increase in its value with the increase of thickness.

The magnitude of the absorption coefficient (α) is relevant to the photon energy of light through the presented relation [18,19]:

$$(\alpha\hbar\omega) = k(\hbar\omega - E_g)^Y \quad (5)$$

where E_g represents Tauc's bandgap, k is constant and dependent on the transition probability, and the exponent, Y, is a constant which takes values of 2 and 1/2, for indirectly allowed and directly allowed transitions, respectively. The values of the optical band gap, E_g , of the $LiCrO_2$ thin film were estimated via Tauc's plot as represented in Fig. 5b. The values of E_g for the $LiCrO_2$ thin films were estimated by extrapolating the straight-line plots to zero absorption. The magnitudes of the direct optical band gap, E_g evaluated via these curves are recorded in Table I. It is obvious that the

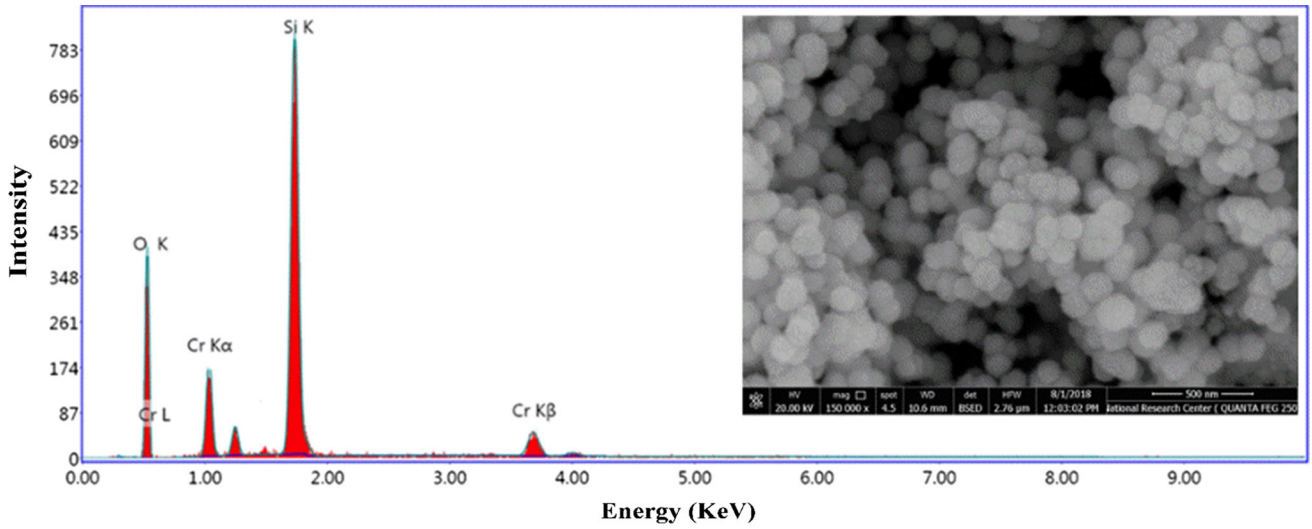

Fig. 3. FE-SEM micrographs and EDX analysis of the $LiCrO_2$ thin film with a thickness of 381 nm.

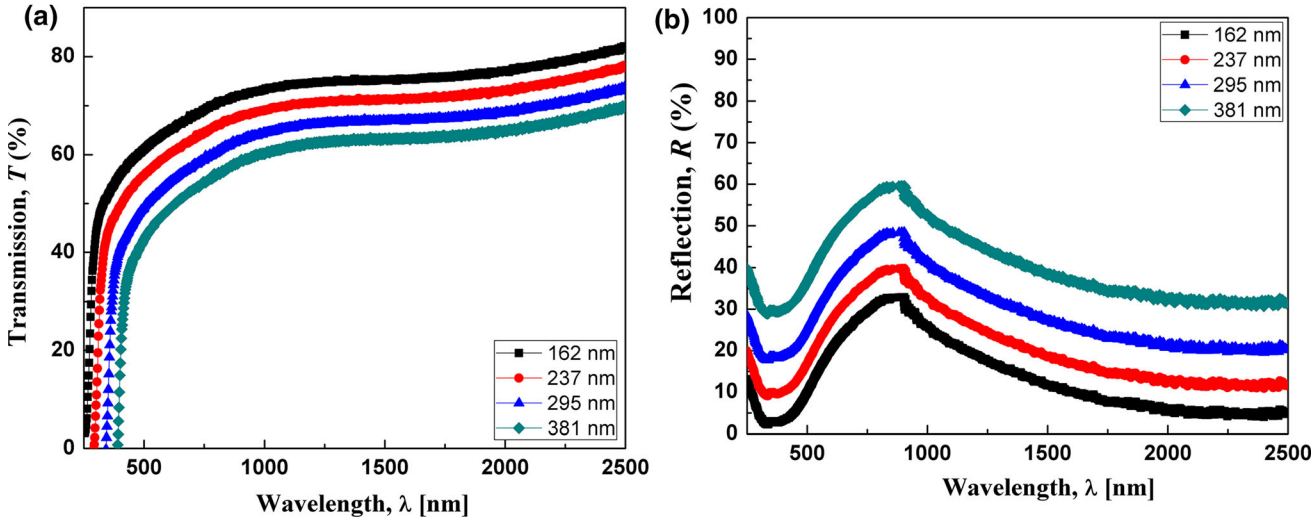

Fig. 4. (a) The transmittance spectra of the $LiCrO_2$ thin films, (b) The reflectance spectra of the $LiCrO_2$ thin films.

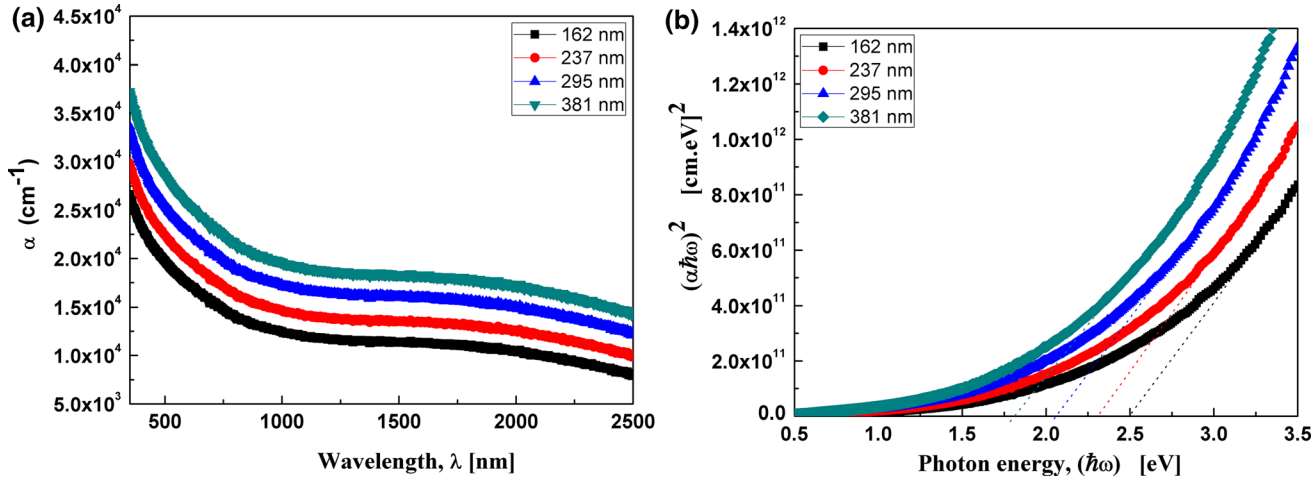

Fig. 5. (a) The dependence of absorption coefficient on the wavelength for the $LiCrO_2$ thin films, (b) Plots of a direct energy gap for the $LiCrO_2$ thin films.

magnitudes of the energy gap decrease from 2.48 eV to 1.81 eV as the thickness increases. This reduction of bandgap is attributed to the increase in the density of defect states due to the increase in film thickness. This allows the states near the conduction band to rise into the forbidden band.[20]

Absorption Index and Refractive Index Characterization

The absorption index (K) of the $LiCrO_2$ films is evaluated by the below expression [21,22]:

$$K = \frac{\alpha\lambda}{4\pi} \tag{6}$$

Figure 6a appearances the behavior of the absorption index (K) of the $LiCrO_2$ films which increases with increasing the film thickness and increasing with increasing the wavelength.

The refractive index, n of the $LiCrO_2$ thin films is given by the presented equation [23,24]:

$$n = \frac{1+R}{1-R} + \left(\frac{4R}{(1-R)^2} - k^2\right)^{1/2} \tag{7}$$

Figure 6b displays the variation of the refractive index, n for the $LiCrO_2$ thin film with wavelength. The plot illustrates that the refractive index of the $LiCrO_2$ thin films exhibits an anomalous dispersion in the wavelength range $\lambda < 1000$ nm. The $LiCrO_2$ thin films exhibit a normal dispersion in the wavelength range $\lambda > 1000$ nm. By increasing the thickness of the $LiCrO_2$ thin films, the magnitude of the refractive index has been increased.

Dispersion Refractive Index Characterization

The dispersion of the refractive index of the $LiCrO_2$ thin films can be predetermined by the Wemple–DiDomenico model.[25,26] This model shows that the refractive index of the $LiCrO_2$ thin films is

related to both the oscillation energy, E_o, and the dispersion energy E_d according to the presented formulas:

$$n^2(h\upsilon) = 1 + \frac{E_d E_o}{\left(E_o^2 - (h\upsilon)^2\right)} \tag{8}$$

where $\hbar\upsilon$ represents photon energy.

The magnitudes of E_o and E_d for the $LiCrO_2$ films were evaluated by plotting the $(n^2-1)^{-1}$ versus the $(\hbar\upsilon)^2$ as illustrated in Fig. 7a. The plot produces straight lines its slope and intercept equal $(E_oE_d)^{-1}$ and (E_o/E_d), respectively.

The dependence of E_o and E_d on the thickness of the $LiCrO_2$ thin films are presented in Fig. 7b. It is observed from the figure that dispersion energy E_d increases with increasing the film thickness while the oscillator energy E_o exhibits a reverse manner to E_d. The other oscillator parameters for the $LiCrO_2$ thin films such as the static refractive index, n_o (0), energy gap in relation to Wemple-DiDomenico E_g^{wmp} and the static dielectric constant, $\varepsilon_s(=n_o^2)$ were evaluated according to the presented relations:[27–30]

$$no = \sqrt{1 + \frac{E_d}{E_o}} \tag{9}$$

$$E_g^{wmp} = \frac{E_o}{2} \tag{10}$$

$$\varepsilon_s = n^2(o) \tag{11}$$

The oscillator parameters for the $LiCrO_2$ films were listed in Table II. It is observed from Table II that the magnitudes of the dispersion parameters E_o, E_d, n_0, ε_s, E_g decrease with the increase in thickness of

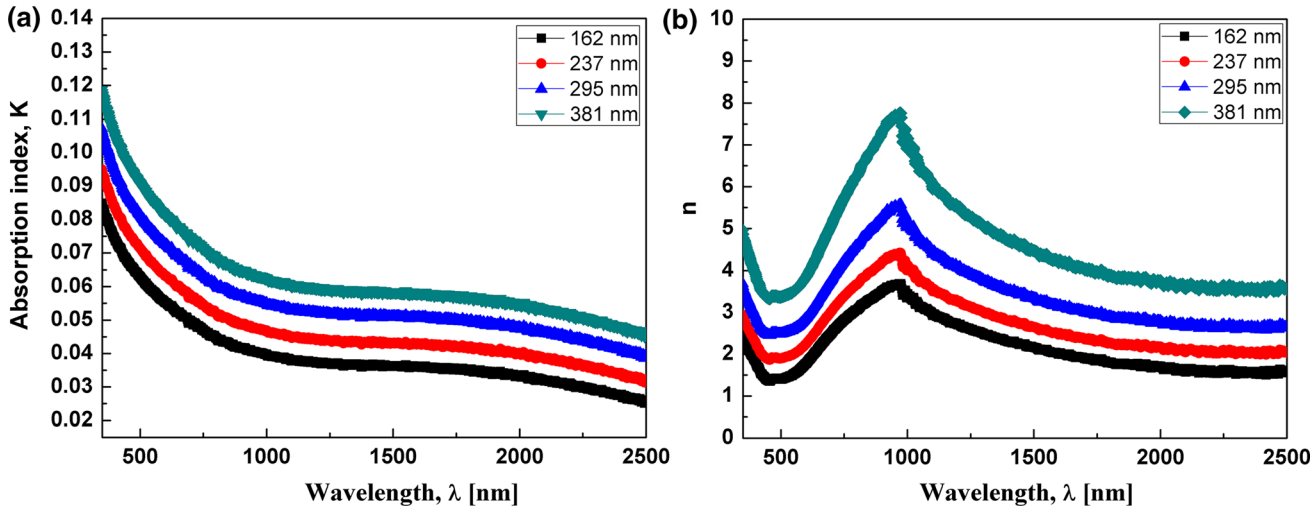

Fig. 6. (a) The variation of the absorption index with the wavelength for the $LiCrO_2$ thin films, (b) The refractive index versus the wavelength for the $LiCrO_2$ thin films.

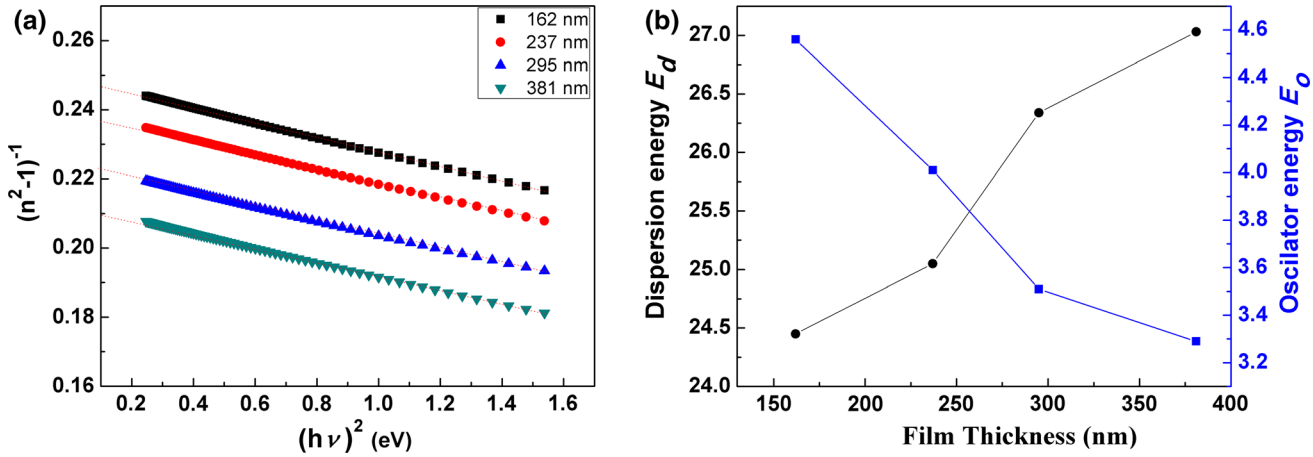

Fig. 7. (a) The dependence of $(n^2-1)^{-1}$ on $(h\upsilon)^2$ for the $LiCrO_2$ thin films, (b) The variation of the E_o and E_d with the thickness of the $LiCrO_2$ thin films.

Table II. The optical band gap and the values of single oscillator parameters for the $LiCrO_2$ thin films

Film thickness, nm	E_g^{dir}, eV	E_d, eV	E_o, eV	n_o	ε_s	M_{-1}, eV^{-2}	M_{-3}, eV^{-2}	E_g^{WD}, eV
162	2.48	24.45	4.56	2.69	5.48	5.37	0.25	2.28
237	2.29	25.05	4.01	2.80	5.29	6.25	0.39	2.01
295	2.07	26.34	3.51	2.83	2.97	7.49	0.61	1.75
381	1.82	27.03	3.29	2.94	2.74	8.20	0.75	1.64

the $LiCrO_2$ films. This could be related to the variant in ionicity bonds. It can be seen that E_o is related to E_g by this expression $E_o \approx 1.8\ E_g$ which agrees with the expectancy of a single oscillator model.

The magnitudes of the optical spectral moments M_{-1} and M_{-3} for the $LiCrO_2$ films were estimated by knowing the E_o and E_d according to the below formulas [31]:

$$M_{-1} = \frac{E_d}{E_o} \tag{12}$$

$$M_{-3} = \frac{M_{-1}}{E_o^2} \tag{13}$$

The magnitudes of the moments for the $LiCrO_2$ films are recorded in Table II. By increasing the thickness of the $LiCrO_2$ thin films, the magnitudes of the optical spectral moments M_{-1} and M_{-3} were increased.

Dielectric Constants, Optical Conductivity and Optical Electronegativity

The dielectric constants of the $LiCrO_2$ thin films can be evaluated from the extinction coefficient k and refractive index n values according to the below expressions [32,33]:

$$\varepsilon_1 = n^2 - k^2 \tag{14}$$

$$\varepsilon_2 = 2nk \tag{15}$$

where ε_1 represents the real part of dielectric constant and ε_2 represents the imaginary part of the dielectric constant for the $LiCrO_2$ thin films.

Figure 8a and b represents the wavelength dependence of ε_1 and ε_2 for the $LiCrO_2$ films. It has been noted that the ε_1 and ε_2 increased with increasing film thickness, and this behavior indicates a good optical response of the material (Fig. 9).

The optical conductivity of the $LiCrO_2$ films has been estimated from the below expression [34,35]:

$$\sigma_{\text{opt}} = \frac{\alpha n c}{4\pi} \tag{16}$$

where c represents the speed of light.

Figure 10b displays the variation of the optical conductivity of $LiCrO_2$ films with photon energy. It is seen from this plot that the optical conductivity increases with increasing film thickness and increases with increasing photon energy for the $LiCrO_2$ films; this performance is related to the increase of electron excitation via increasing the magnitude of the photon energy.

Optical electronegativity is an important parameter showing the tendency of an atom to attract an electron from the anionic band. It is used to evaluate the difference of physicochemical parameters of the materials. The optical electronegativity can be evaluated by the below formula [36]:

$$\eta_{opt} = \left[\frac{A}{n}\right]^{1/4} \tag{17}$$

where n is the refractive index and A is dimensionless constant which has the value 25.54 for all materials. Figure 10a represents the variation of optical electronegativity with the photon energy of the $LiCrO_2$ thin films. The values of optical electronegativity were decreased with the increase in photon energy. The decrease in the magnitude of η_{opt} with the increase in film, thickness confirms the increase in the three-dimensional network in the film.

Nonlinear Optical Properties

The nonlinear optical parameters of the prepared material like the nonlinear refractive index n_2 and the third-order nonlinear susceptibility $\chi^{(3)}$ are important to study the possibility of using it in the fabrication of frequency conversion and optical switching devices, and different photonic applications. Both n_2 and $\chi^{(3)}$ are important parameters needed to study the nonlinear optical properties of the $LiCrO_2$ films. The magnitude of the $\chi^{(3)}$ for the $LiCrO_2$ thin films has been evaluated by the following formula [37,38]:

$$\chi^{(3)} = B\left[\frac{n_0^2 - 1}{4\pi}\right]^4 \tag{18}$$

where n_0 is the value of the static refractive index, B is a constant factor equal 1.7×10^{-10} esu. The magnitude of n_0 was calculated via intercept of the plot between $(n^2-1)^{-1}$ versus $(h\nu)^2$ for the $LiCrO_2$ films. The obtained magnitudes of n_0 for the $LiCrO_2$ films were tabulated in Table III.

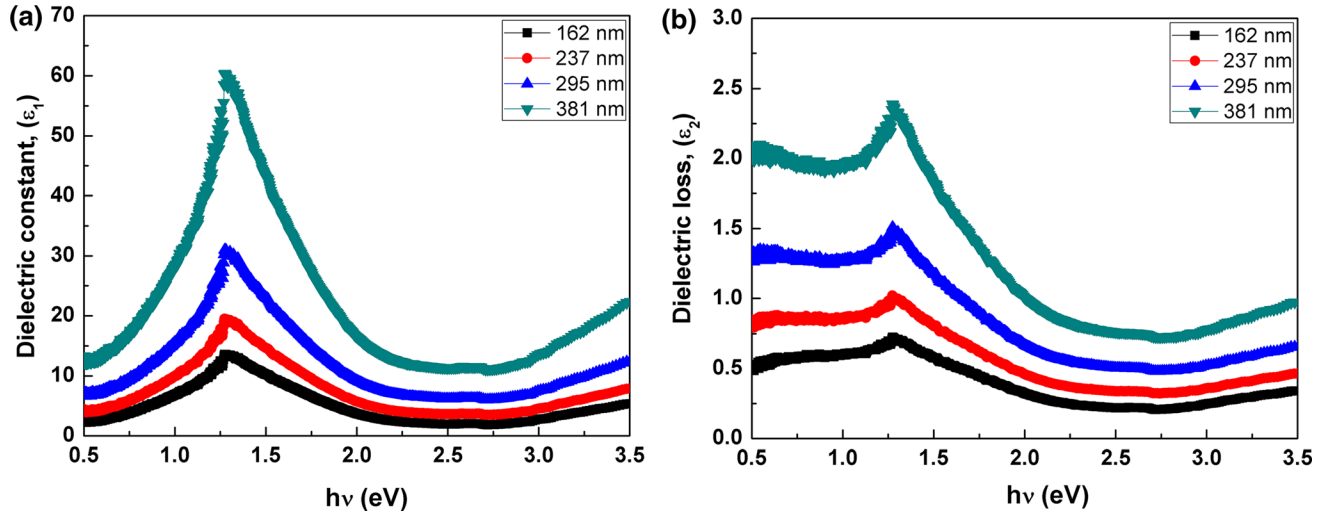

Fig. 8. (a) Plots of the real dielectric constant with the photon energy for the $LiCrO_2$ thin films, (b) The variation of the imaginary dielectric constant as a function of photon energy for the $LiCrO_2$ thin films.

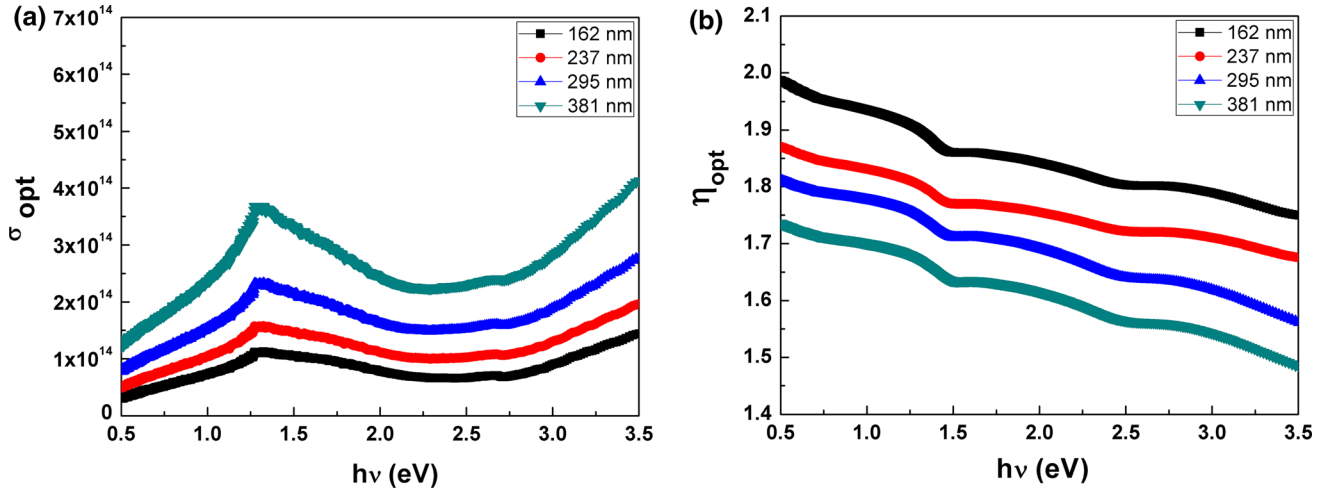

Fig. 9. (a) The optical conductivity of the $LiCrO_2$ thin films as a function of photon energy $(h\nu)$, (b) The dependence of electronegativity on the photon energy $(h\nu)$ for the $LiCrO_2$ thin films.

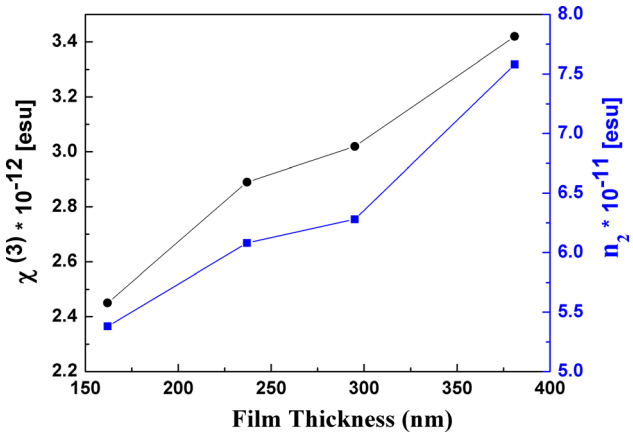

Fig. 10. The dependence of third-order nonlinear optical susceptibility $\chi^{(3)}$ and nonlinear refractive index n_2 on the thickness of the $LiCrO_2$ thin films.

The nonlinear refractive index n_2 of the $LiCrO_2$ thin films has been estimated by the presented formula [39,40]:

$$n_2 = \frac{12\pi\chi^{(3)}}{n_0} \tag{19}$$

The magnitudes of both $\chi^{(3)}$ and n_2 for the $LiCrO_2$ thin films are recorded in Table III. It can be noticed that both parameters were increased by increasing the film thickness. The large values of the obtained nonlinear parameters make our investigated material a good candidate in the fabrication of low-power devices for telecommunication applications.

CONCLUSION

In this study, high-quality $LiCrO_2$ thin films were prepared through a simple spray pyrolysis system at different thicknesses (162 nm, 237 nm, 295 nm

Table III. The nonlinear optical parameters for the $LiCrO_2$ thin films

Film thickness, nm	$^{(3)} \times 10^{-12}$, esu	$n_2 \times 10^{-11}$, esu
162	2.45	5.38
237	2.89	6.081
295	3.019	6.28
381	3.42	7.58

and 381 nm). The x-ray analysis of the $LiCrO_2$ thin films shows that the as-deposited $LiCrO_2$ films are polycrystalline in nature with the rhombohedral crystal structure. The linear and dispersion optical parameters of the $LiCrO_2$ thin films were evaluated in the spectral range 400–2500 nm. The type of optical transition in the $LiCrO_2$ thin films was detected to be a direct allowed transition. The dispersion refractive index data of the $LiCrO_2$ thin films were analyzed according to the single oscillator model to evaluate the dispersion parameters including the dispersion energy, the static refractive index and the oscillator energy. The optoelectrical and nonlinear optical parameters like optical conductivity, third-order nonlinear susceptibility, optical electronegativity and the nonlinear refractive index of the $LiCrO_2$ thin films were evaluated.

REFERENCES

1. M.S. El-Bana, I.M. El Radaf, S.S. Fouad, and G.B. Sakr, *J. Alloys Compd.* 705, 333 (2017).
2. K.-S. Han, S.-W. Song, S. Tsurimoto, H. Fujita, I. Sasagawa, K.-H. Choi, H.-K. Kang, and M. Yoshimura, *Solid State Ionics* 151, 11 (2002).
3. M.M. Ahmad, *RSC Adv.* 5, 25824 (2015).
4. J. Huang, J. Yang, W. Li, W. Cai, and Z. Jiang, *Thin Solid Films* 516, 3314 (2008).
5. M. Yoshimura, K.-S. Han, and S. Tsurimoto, *Solid State Ion.* 106, 39 (1998).
6. C.-J. Kim, I.-S. Ahn, K.-K. Cho, S.-G. Lee, and J.-K. Chung, *J. Alloys Compd.* 449, 335 (2008).
7. P. Fragnaud and D.M. Schleich, *Ionics (Kiel).* 1, 183 (1995).
8. M.Y. Song and R. Lee, *J. Power Sour.* 111, 97 (2002).
9. X. Lai, D. Gao, J. Bi, Y. Li, P. Cheng, C. Xu, and D. Lin, *J. Alloys Compd.* 487, L30 (2009).
10. F. Michalak, K. Von Rottkay, T. Richardson, J. Slack, and M. Rubin, *Electrochim. Acta* 44, 3085 (1999).
11. X. Zheng, X. Li, Z. Wang, H. Guo, Z. Huang, G. Yan, and D. Wang, *Electrochim. Acta* 191, 832 (2016).
12. T.A. Hameed, I.M. El Radaf, and H.E. Elsayed-Ali, *J. Mater. Sci. Mater. Electron.* 29, 12584 (2018).
13. I.M. El Radaf, S.S. Fouad, A.M. Ismail, and G.B. Sakr, *Mater. Res. Express* 5, 46406 (2018).
14. X. Wang, T. Liu, H. Guan, F. Yu, and H. Hou, *Optoelectron. Adv. Mater. Commun.* 9, 1190 (2015).
15. M.S. AlKhalifah, I.M. El Radaf, and M.S. El-Bana, *J. Alloys Compd.* 813, 152169 (2020).
16. I.S. Yahia, I.M. El Radaf, A.M. Salem, and G.B. Sakr, *J. Alloys Compd.* 776, 1056 (2019).
17. A.S. Hassanien and I. Sharma, *J. Alloys Compd.* 798, 750 (2019).
18. K. Shen, C. Ou, T. Huang, H. Zhu, J. Li, Z. Li, and Y. Mai, *Sol. Energy Mater. Sol. Cells* 186, 58 (2018).
19. M. Shkir, A. Khan, A.M. El-Toni, A. Aldalbahi, I.S. Yahia, and S. AlFaify, *J. Phys. Chem. Solids* 130, 189 (2019).
20. T.A. Hameed, I.M. El Radaf, and G.B. Sakr, *Appl. Phys. A* 124, 684 (2018).
21. T.A. Hameed, A.R. Wassel, and I.M. El Radaf, *J. Alloys Compd.* 805, 1 (2019).
22. A.M. Mansour and I.M. El Radaf, *Int. J. Microstruct. Mater. Prop.* 14, 419 (2019).
23. I.M. El Radaf, T.A. Hameed, G.M. El Komy, and T.M. Dahy, *Ceram. Int.* 45, 3072 (2019).
24. P. Sharma, M.S. El-Bana, S.S. Fouad, and V. Sharma, *J. Alloys Compd.* 667, 204 (2016).
25. S.H. Wemple, *Phys. Rev. B* 7, 3767 (1973).
26. S.H. Wemple and M. DiDomenico Jr, *Phys. Rev. B* 3, 1338 (1971).
27. I.M. El Radaf and R.M. Abdelhameed, *J. Alloys Compd.* 765, 1174 (2018).
28. V. Pawar, M. Kumar, P.K. Dubey, M.K. Singh, A.S.K. Sinha, and P. Singh, *Appl. Phys. A* 125, 10 (2019).
29. A. El-Denglawey, M.M. Makhlouf, and M. Dongol, *Results Phys.* 10, 714 (2018).
30. A. Saeed and I. Sharma, *Opt. Int. J. Light Electron Opt.* 200, 163415 (2020).
31. R.R. Reddy, K.R. Gopal, K. Narasimhulu, L.S.S. Reddy, K.R. Kumar, C.V.K. Reddy, and S.N. Ahmed, *Opt. Mater. (Amst).* 31, 209 (2008).
32. E.R. Shaaban, N. Afify, and A. El-Taher, *J. Alloys Compd.* 482, 400 (2009).
33. E.R. Shaaban, M.N. Abdel Salam, M. Mohamed, M.A. Abdel-Rahim, and A.Y. Abdel-Latief, *J. Mater. Sci. Mater. Electron.* 28, 13379 (2017).
34. S.S. Fouad, I.M. El Radaf, P. Sharma, and M.S. El-Bana, *J. Alloys Compd.* 757, 124 (2018).
35. I.M. El Radaf, T.A. Hameed, and I.S. Yahia, *Mater. Res. Express* 5, 66416 (2018).
36. S. Gedi, V.R.M. Reddy, C. Park, J. Chan-Wook, and K.T.R. Reddy, *Opt. Mater. (Amst).* 42, 468 (2015).
37. A.A.A. Darwish, M. Rashad, A.E. Bekheet, and M.M. El-Nahass, *J. Alloys Compd.* 709, 640 (2017).
38. R.M. Abdelhameed and I.M. El Radaf, *Mater. Res. Express* 5, 66402 (2018).
39. S.R. Alharbi, A.A.A. Darwish, S.E. Al Garni, H.I. El Saeedy, and K.F.A. El-Rahman, *Infrared Phys. Technol.* 78, 77 (2016).
40. V. Ganesh, L. Haritha, M. Anis, M. Shkir, I.S. Yahia, A. Singh, and S. AlFaify, *Solid State Sci.* 86, 98 (2018).